第 36 卷第 4 期
2020 年 4 月

无 机 化 学 学 报
CHINESE JOURNAL OF INORGANIC CHEMISTRY

Vol.36 No.4
737-746

非晶态铁基固体碱催化剂的酯交换性能

吴辰亮　李小青　张荷丰　严新焕*
(浙江工业大学绿色化学合成技术国家重点实验室培育基地,杭州　310014)

摘要：通过化学还原法和共沉淀法分别制备了非晶态和晶态的 $FeCeO_x/SiO_2$ 固体碱催化剂。与晶态的 $FeCeO_x/SiO_2$ 相比,非晶态的 $FeCeO_x/SiO_2$ 催化剂对梨醇酯与甲醇的酯交换活性显著提高。通过电感耦合等离子体质谱(ICP-MS)、N_2 吸附–脱附、透射电子显微镜(TEM)结合选区电子衍射(SAED)、X 射线衍射(XRD)、X 射线光电子能谱(XPS)、CO_2-TPD 和 NH_3-TPD 等对催化剂进行表征。结果表明催化剂的活性与其碱性密切相关，非晶态 $FeCeO_x/SiO_2$ 显示出相对于晶态 $FeCeO_x/SiO_2$ 更强的碱性。使用非晶态 $FeCeO_x/SiO_2$ 催化剂进行梨醇酯酯交换反应,在 130 ℃下反应 10 h,梨醇酯的转化率达到 95%,异戊烯醇的选择性达到 96%。在重复使用 10 次后,催化剂活性基本不变。对新鲜的和套用 10 次后的 $FeCeO_x/SiO_2$ 催化剂进行 X 射线衍射分析,表明该催化剂在套用 10 次后仍未晶化,证实其具有良好的稳定性,说明该催化剂在非均相催化酯交换反应中具有应用价值。

关键词：$FeCeO_x/SiO_2$；固体碱；非晶态；酯交换
中图分类号：O643.36　　**文献标识码**：A　　**文章编号**：1001-4861(2020)04-0737-10
DOI:10.11862/CJIC.2020.078

Transesterification Performance of Amorphous Iron-Based Solid Base Catalyst

WU Chen-Liang　LI Xiao-Qing　ZHANG He-Feng　YAN Xin-Huan*
(*State Key Laboratory Breeding Base of Green Chemistry-Synthesis Technology, Zhejiang University of Technology, Hangzhou* 310014, *China*)

Abstract: Both amorphous and crystalline $FeCeO_x/SiO_2$ solid base catalysts were prepared by chemical reduction and co-precipitation methods, respectively. The activity of amorphous $FeCeO_x/SiO_2$ for the transesterification of prenyl acetate with methanol was remarkably enhanced compared with crystalline $FeCeO_x/SiO_2$. The catalysts were characterized by inductively coupled plasma mass spectrometry (ICP-MS), N_2 adsorption-desorption, transmission electron microscopy (TEM) in combination with selected area electron diffraction (SAED), X-ray diffraction (XRD), X-ray photoelectron spectroscopy (XPS), and temperature programmed desorption (CO_2-TPD and NH_3-TPD). As a result, the activity of the catalysts is found to be closely related to its basicity, and the amorphous $FeCeO_x/SiO_2$ shows higher basicity. Prenyl acetate conversion of 95% and prenyl alcohol selectivity of 96% were obtained using amorphous $FeCeO_x/SiO_2$ catalyst in transesterification reaction at 130 ℃ for 10 h. The catalyst maintained a high level of activity after 10 cycles of testing. X-ray diffraction analyses of fresh and used $FeCeO_x/SiO_2$ catalyst demonstrated that this catalyst is exceptionally stable, which could be of value in industrial application related to heterogeneous catalytic transesterification.

Keywords: $FeCeO_x/SiO_2$; solid base; amorphous; transesterification

收稿日期:2019-07-23。收修改稿日期:2019-12-26。
国家重点研发计划(No.2017YFC0210900)资助项目。
*通信联系人。E-mail:xhyan@zjut.edu.cn

0 Introduction

Maintaining low environment impacts in industrial processes has become one of the major issues of sustainable chemistry. Thus, solid bases have been widely used in chemical industry to solve it. They are proposed as heterogeneous catalysts for a variety of processes such as aldol condensation, olefin isomerization, Guerbet condensation, epoxide ring-opening, production of fatty acid methyl esters from natural fats, NO_x adsorption and reaction, transesterification of esters and alcohols[1-3]. The replacement of liquid acids and bases with solid acids and bases in organic reactions makes sense because it combines the advantages of less environmental hazard, easier separation from the reaction mixture, and ease of recycling[4-6]. At the industrial scale, a homogeneous catalyst such as KOH or NaOH is often used to promote the transesterification of the prenyl acetate to produce prenyl alcohol[7]. It requires water washing to remove dissolved catalyst from product and suffers from separation problems. Thus, heterogeneous catalysts become competitive candidates because they can avoid these problems.

A large number of crystalline iron solid base catalysts have been investigated for transesterification reactions, especially in the transesterification to biodiesel productions. Macala et al.[8] prepared an iron-doped hydrotalcite with adjustable properties, in which Fe^{3+} ions replaced some of Al^{3+} in the Mg/Al layered double hydroxide lattice. Various types of iron doped catalysts such as iron doped zinc oxide catalysts[9], iron doped carbonaceous catalysts[10] and iron oxide supported on silica[11] were studied for the production of biodiesel. In order to enhance the basicity of catalysts, Mg-Fe mixed oxide[12] and Ca-Fe mixed oxide[13] were also commonly used in the production of biodiesel. However, the activity of the catalysts decreased significantly after several uses attributed to the leaching of the Ca or Mg component. Moreover, Shi et al.[14] compared different crystal forms of Fe_2O_3 and found stronger magnetism could increase the rate of biodiesel transesterification. Ce-Fe mixed oxides were also used in the transesterification of dimethyl carbonate and phenol[15], propylene carbonate and methanol[16], indicating its universality in various transesterification reactions. However, in the crystalline iron-based catalyst, both of Mg-Fe and Ca-Fe had shown excellent transesterification activity but with poor stability due to the leaching of active component. Ce-Fe had the advantage of high stability. However, several shortcoming of Ce-Fe catalysts need to be addressed, including the weak basicity and poor activity.

Herein, we prepared amorphous $FeCeO_x/SiO_2$ and crystalline $FeCeO_x/SiO_2$ to compare their transesterification activity. Previous studies showed that the surface acid and base functionalities played a major role in transesterification reaction[17-18]. Amorphous $FeCeO_x/SiO_2$ catalyst was prepared by first reduction and oxidation. Fe and Ce formed an amorphous structure during the reduction process, and a large amount of basic sites were formed during the oxidation process. The characterization results showed that the amorphous $FeCeO_x/SiO_2$ had more basic sites than the crystalline $FeCeO_x/SiO_2$. Moreover, the interaction of Ce with Fe enhanced the stability of the catalyst[19]. The aim of this study is to evaluate the catalytic behavior of amorphous and crystalline $FeCeO_x/SiO_2$ in the transesterification reaction of prenyl acetate.

1 Experimental

1.1 Materials

$Fe(NO_3)_3\cdot 9H_2O$, $Ce(NO_3)_3\cdot 6H_2O$ and prenyl acetate (AR) were purchased from ShanghaiAladdin Bio-Chem Technology Co., Ltd. SiO_2, methanol (AR), K_2CO_3, KOH and KBH_4 were purchased from Shanghai Macklin Biochemical Co., Ltd.

1.2 Catalyst preparation

According to the literatures[20-21], an appropriate amount of Ce could not only increase the basic sites of the catalyst, but also improved the stability of the catalyst through the interaction between Fe and Ce. However, excessive Ce blocked the pores and reduced the surface area of the catalyst. Excessive Fe formed agglomeration with Ce, thus requiring a suitable ratio

of Fe to Ce (w_{Fe}/w_{Ce}). After preliminary experiments to determine the metal ratio of Fe and Ce, the crystalline $FeCeO_x/SiO_2$ with 5%(w/w) Fe metal and 10%(w/w) Ce metal was prepared by co-precipitation method. The solution of water and ethanol were mixed with 1 mol·L^{-1} solution of $Fe(NO_3)_3 \cdot 9H_2O$ and $Ce(NO_3)_3 \cdot 6H_2O$ under vigorous stirring. The 1 mol·L^{-1} K_2CO_3 aqueous solution was used as a precipitant adding dropwise at a constant rate to precipitating batch, maintaining the pH constant (at 8.0) during precipitation and temperature was kept at 303 K. Obtained precipitate was aged for 1 h with the mother liquors still under stirring at the reaction temperature. Then, the precipitate was filtered out and washed with successive portions of 250 mL distilled water and 250 mL methanol. The precipitate were dried in static air at 333 K for 5 h. The catalyst was obtained by calcination under ambient air at 673 K for 5 h.

The amorphous $FeCeO_x/SiO_2$ with 5% Fe metal and 10% Ce metal was prepared by chemical reduction under vigorous stirring from 1 mol·L^{-1} solution of $Fe(NO_3)_3 \cdot 9H_2O$ and $Ce(NO_3)_3 \cdot 6H_2O$, the solution mixed of water and ethanol. The KBH_4 solution ($n_{BH_4^-}$:($n_{Fe}+n_{Ce}$) =2.5∶1) as a reducing agent was added dropwise at a constant rate and temperature was kept at 303 K, maintaining the pH constant (at 8.0) by KOH during reduction. After the addition was completed, the precipitate was aged for 1h then filtered out. Then the precipitate was washed with 250 mL distilled water and 250 mL methanol. The catalyst was re-oxidized by static air at 333 K for 5 h. According to metal mass ratio, the as-synthesized catalyst was denoted as 5% Fe10%CeO_x/SiO_2-M (M=C or A for crystalline or amorphous structure, respectively).

1.3 Catalysts characterization

The metal element content of the catalyst was determined using Agilent 7500CE inductively coupled plasma mass spectrometry (ICP-MS).

N_2 adsorption at −196 ℃ was measured using a Micromeritics ASAP 2010 system, the samples were degassed at 200 ℃ for 6h under high vacuum. The surface area was calculated by using the Brunauer-Emmett-Teller (BET) method. The total pore volume was determined by nitrogen adsorption at a relative pressure of 0.99, and the pore size distributions were calculated from the nitrogen adsorption isotherms by the Barrett-Joyner-Hallenda(BJH) method.

Transmission electron microscopy (TEM) experiments were conducted on a JEOL JEM-1200EX electron microscope with an accelerating voltage of 60 kV. Before being transferred into the TEM chamber, the samples dispersed in ethanol were deposited onto holey carbon films supported on Cu grids.

XRD data were acquired with a Rigaku D/Max-2500/PC powder diffraction system, using Cu $K\alpha$ (λ= 0.154 06 nm) radiation at 40 kV and 100 mA. The step size was 5° over the 2θ range of 5°~80°.

XPS data were acquired using an A Kratos AXIS Ultra DLD photoelectron spectrometer with monochromatic Al $K\alpha$ (1 486.6 eV) radiation under ultra-high vacuum. The binding energy (BE) values were calibrated internally using the C1s peak with BE= 284.8 eV. The experimental error was within ±0.1 eV. An approximate quantitative calculation was made by integrating the areas of the Ce^{3+} and Ce^{4+} peaks after curve peak fitting.

CO_2/NH_3-TPD data were acquired using a Builder PCA-1200 chemical adsorption instrument. Each sample was pretreated in a He flow at 373 K for 1 h and then cooled to room temperature. CO_2/NH_3 was adsorbed at room temperature for 30 min at 40 mL·min^{-1}, after which a He flow was initiated to purge residual CO_2/NH_3 for 30 min. The desorption was performed at a heating rate of 10 K·min^{-1} from 323 to 973 K, using a thermal conductivity detector and He as the carrier gas.

1.4 Catalytic test

The transesterification reactions of prenyl acetate with methanol were carried out in 500 mL stainless steel autoclave equipped with a magnetic stirrer. 15 mL of prenyl acetate and 135 mL of methanol were mixed well, followed by the introduction of 0.6 g of the catalyst. The reactor was pressurized with N_2 to 0.5 MPa and heated to 130 ℃ under stirring for 10 h. After the reaction, the autoclave was cooled down in ice water and the mixture was centrifuged and

analyzed by a GC equipped with a DB-5 capillary column coupled with a FID detector. In the transesterification of prenyl acetate with methanol, prenyl alcohol and methyl acetate were the target molecule and co-product, respectively. In addition to the main products, 3-methyl-3-methoxy-1-butene and 1-methoxy-3-methyl-2-butene were by-product. The conversion (Conv.) of prenyl acetate and selectivity (Sel.) to prenyl alcohol were calculated as follows:

$$\text{Conversion}=\frac{m_1/M_1-m_2/M_1}{m_1/M_1}\times 100\%$$

$$\text{Selectivity}=\frac{m_3/M_2}{m_1/M_1-m_2/M_1}\times 100\%$$

where m_1 is the mass of prenyl acetate in the feed, m_2 is the mass of prenyl acetate in the product, m_3 is the mass of prenyl alcohol generated, M_1 is the molar mass of prenyl acetate, and M_2 is the molar mass of prenyl alcohol.

2 Results and discussion

2.1 Characterization results

Table 1 showed the metal loading and textural properties of prepared 5% Fe10% CeO_x/SiO_2 catalysts, as well as SiO_2. It could be seen that the actual loading was slightly lower than the theoretical value, indicating that some metal loss may occur during the preparation step. However, these losses had little effect on the catalyst and could be neglected. Therefore, the actual mass ratio could be replaced by a theoretical value. According to N_2 adsorption-desorption results, SiO_2 exhibited the largest surface area of 194 $m^2\cdot g^{-1}$ after loading the metal. The surface area and average pore volume decreased owning to the blockage of narrow pores by the introduction of large amount of Fe and Ce species.

Fig.1 showed the morphology images of 5% Fe10% CeO_x/SiO_2-C and 5% Fe10% CeO_x/SiO_2-A. It revealed that the 5% Fe10% CeO_x/SiO_2-C was nearly uniform with good dispersity and crystal structures. 5%Fe10%CeO_x/SiO_2-A exhibited only a densely packed amorphous matrix, while the Fe and Ce oxide phases were homogeneously mixed at quasi-molecular level and formed a prevalently amorphous structure. Solid solution-like $FeCeO_x$ species may be present in amorphous samples. In the selected area electron diffraction(SAED) mode, the crystalline catalyst showed a circle of diffracted aura, while the amorphous catalyst showed a diffuse halo, due to the amorphous structure.

Fig.2 illustrated XRD patterns of the $FeCeO_x/SiO_2$ catalysts. A very broad peak at 2θ of *ca.* 22.0° was clearly observed on both catalysts, which can be ascribed to amorphous SiO_2 (PDF No.29-0085) [22]. Diffraction peaks of CeO_2 phase were only observed at 2θ=28.1°, 33.1°, 47.5°, 56.5° in the sample prepared by co-precipitation, which was characteristic of a cubic fluorite-structured material (PDF No.81-0792)[23]. The peaks belonging to Fe_2O_3 were not observed, likely referring to its low content. In the sample prepared by chemical reduction, no diffraction peaks of Fe or Ce were observed. The TEM and XRD results confirm that the catalyst prepared by chemical reduction exists in some amorphous state.

XPS measurements were used to characterize the surface element composition of the resultant $FeCeO_x/SiO_2$ (Fig.3). It revealed that the surface of $FeCeO_x/SiO_2$ contained mainly Si and O with a bit amount of Fe and Ce. To determine the chemical components and the oxidation states of each element (Fe, Ce), high-resolution XPS spectra of Fe2*p* and Ce3*d* were

Table 1 Physicochemical characterizations of as-prepared catalysts

Catalyst	Actual load of Fe[a] / %	Actual load of Ce[a] / %	S_{BET} / ($m^2\cdot g^{-1}$)	Pore diameter[b] / nm	Pore volume[c] / ($cm^3\cdot g^{-1}$)
SiO_2	—	—	194	14.38	1.38
5%Fe10%CeO_x/SiO_2-A	4.9	9.7	153	15.78	1.13
5%Fe10%CeO_x/SiO_2-C	4.8	9.5	189	13.35	1.21

[a] Determined by the ICP-MS technique; [b] Average pore diameter; [c] BJH desorption pore volume.

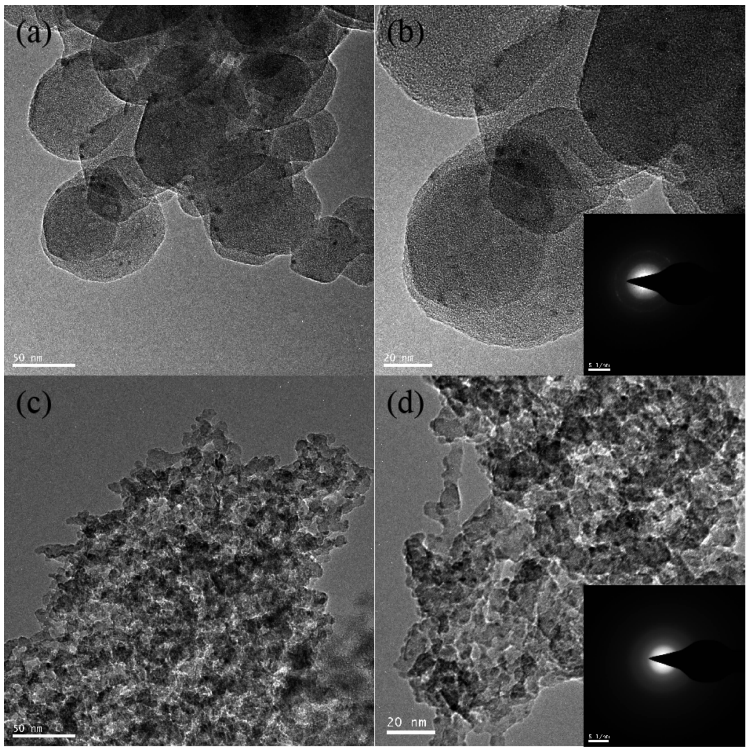

Fig.1　TEM images of $FeCeO_x/SiO_2$ samples: (a, b) 5%Fe10%CeO_x/SiO_2-C, (c, d) 5%Fe10%CeO_x/SiO_2-A

highlighted. O1*s* spectra was used to illustrate the basic site on catalyst surface.

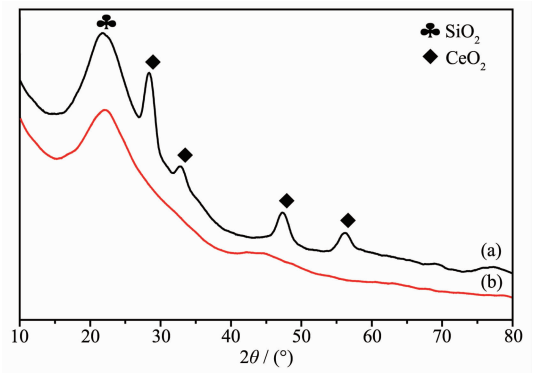

Fig.2　XRD patterns of $FeCeO_x/SiO_2$ samples: (a) 5%Fe 10%CeO_x/SiO_2-C, (b) 5%Fe10%CeO_x/SiO_2-A

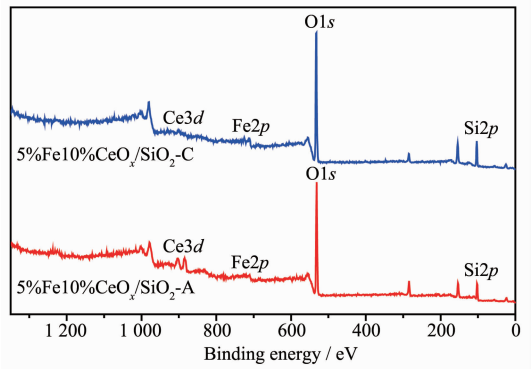

Fig.3　XPS spectra of $FeCeO_x/SiO_2$ samples

The spectra of Fe2*p* (Fig.4) from $FeCeO_x/SiO_2$ indicated the existence of doublet Fe2$p_{3/2}$ and Fe2$p_{1/2}$ with binding energies of about 711.0 and 724.6 eV, respectively[24-25]. There was satellite peak situated at about 718.8 eV, which was a major characteristic of Fe^{3+} [26]. Fe2*p* spectra of the two catalysts were almost the same, clearly revealed that most of the Fe on the surface of amorphous catalyst were oxidized to Fe^{3+}.

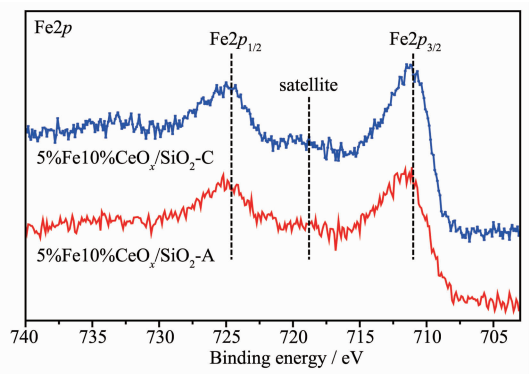

Fig.4　XPS spectra of Fe2*p* of $FeCeO_x/SiO_2$ samples

Fig.5 represents the XPS spectra of Ce3*d* of $FeCeO_x/SiO_2$ catalysts. The Ce3*d* spectra showed a complex multiple peaks. XPS peaks denoted as U‴ (916.7 eV), U″ (907.5 eV), and U (901.0 eV) and V‴

(898.4 eV), V″ (888.2 eV), and V (882.5 eV) are attributed to Ce^{4+} species while U′ (903.5 eV), U_0 (898.8 eV), V′ (884.9 eV), and V_0 (880.3 eV) are assigned to Ce^{3+} species. The peaks assigned U′, U_0, V′, and V_0 are the main representatives of the $3d^{10}4f^1$ electronic state of Ce^{3+} ions, while the peaks assigned U‴, U″, U, V‴, V″ and V are the main representatives of the $3d^{10}4f^0$ electronic state of Ce^{4+} ions[27-28]. The Ce^{3+} relative surface ratio of amorphous and crystalline catalysts was calculated as 82% and 37%, respectively. The increasing amount of Ce^{3+} was due to the different degrees of catalyst oxidation.

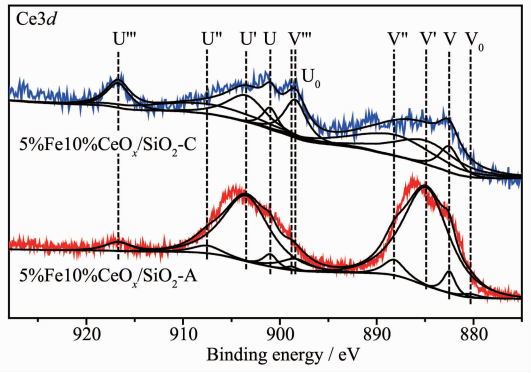

Fig.5 XPS spectra of Ce3*d* of $FeCeO_x/SiO_2$ samples

As presented in Fig.6, two kinds of surface oxygen species were identified by performing a peak-fitting deconvolution. The peaks at higher binding energy of 531.0~533.0 eV are attributed to the surface -OH species (O_α), and the peaks at lower binding energy of 529.0~531.0 eV are characteristic of O^{2-} (O_β), attributed to carbonate species[29-30]. The O_α relative surface ratio in amorphous catalyst (91.9%) was higher than that in crystalline catalyst (90.6%). This indicates that there are more surface -OH species on the surface of the amorphous catalyst, which may lead to more weak basic sites on the catalyst surface.

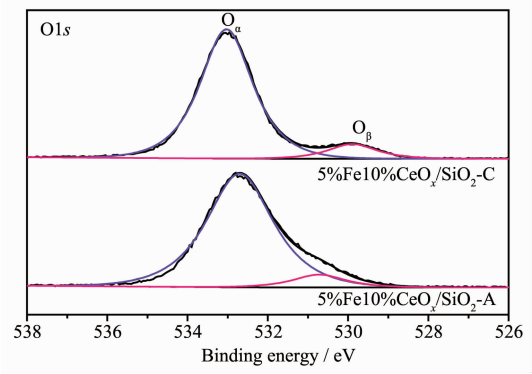

Fig.6 XPS spectra of O1*s* of $FeCeO_x/SiO_2$ samples

From previous work it appeared that the amount of basic sites of the catalyst is an important factor affecting its catalytic activity in the transesterification reaction[31-32]. CeO_2 was a weakly basic oxide, and the addition of Fe enhanced its basicity. In order to prove that the basicity of the catalyst plays a dominant role in this reaction, CO_2-TPD profile and NH_3-TPD profile of catalysts were acquired and shown in Fig.7 (a,b). Peaks in the CO_2/NH_3-TPD profiles were classified as corresponding to: weak (<200 ℃), moderate (200~450 ℃) and strong (>450 ℃) basic/acid sites in the relative temperature. For the CO_2-TPD results, both crystalline and amorphous sample showed significant CO_2 uptake. According to literature[33], CeO_2 showed a weakly basic peak at around 100 ℃, while in the amorphous sample, the intensity of weak and moderate basic sites increased. The intensity of the weak and moderate basic sites depends on the Lewis acid-basic paring

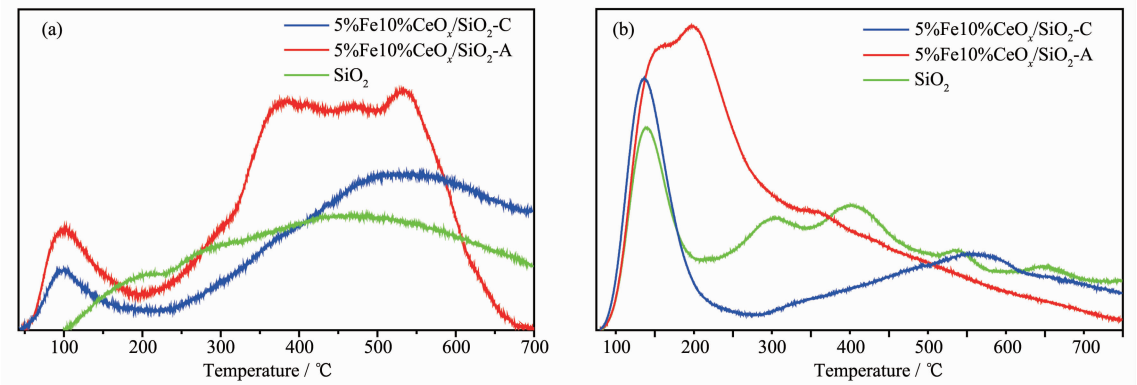

Fig.7 Profiles of CO_2-TPD (a) and NH_3-TPD (b) for as-prepared catalysts

and OH^- bond present on the surface, and the higher basic nature is due to the low coordination of surface O^{2-}[34]. The amount of total basic sites was calculated (Table 2). Thereafter, the basic site density was calculated by dividing the amount of total basic sites per unit mass by the BET surface area[35]. The total amount of CO_2 desorbed from SiO_2, 5%Fe10%CeO_x/SiO_2-A and 5%Fe10%CeO_x/SiO_2-C was 0.85, 2.10 and 1.52 mmol·g^{-1}, respectively. The respectively value of basic site density was: 4.39, 13.74 and 8.06 μmol·m^{-2}. The results in Table 2 indicate that the amorphous catalyst has much more basic sites than the crystalline catalyst.

NH_3 desorption temperature and amount acid sites were calculated (Table 3). The total amount of NH_3 desorbed from SiO_2, 5%Fe10%CeO_x/SiO_2-A and 5%Fe10%CeO_x/SiO_2-C was 0.96, 2.19 and 0.59 mmol·g^{-1}, respectively. The respectively value of acidic site density was: 4.96, 14.33 and 3.13 μmol·m^{-2}. It can be seen that the amorphous catalyst had both basic and acidic sites, and SiO_2 also exhibited a small amount of basicity and acidity. Although SiO_2 had more acid sites than crystalline catalyst, its reaction performance was much worse. The crystalline catalyst had higher activity than SiO_2 due to its stronger basicity. Therefore, this could explain that in the transesterification reaction of prenyl acetate, the activity of the catalyst was mainly derived from the basic site rather than acidic site.

Table 2　TPD analysis using absorbed CO_2 for determining the basic properties of as-prepared catalysts

Catalyst	TPD analysis of absorbed CO_2 / (mmol·g^{-1})			Total evolved CO_2 / (mmol·g^{-1})	Basic site density / (μmol·m^{-2})
	Weak (<200 ℃)	Moderate (200~450 ℃)	Strong (>450 ℃)		
SiO_2	0.05	0.38	0.42	0.85	4.39
5%Fe10%CeO_x/SiO_2-A	0.23	0.94	0.93	2.10	13.74
5%Fe10%CeO_x/SiO_2-C	0.13	0.44	0.95	1.52	8.06

Table 3　TPD analysis using absorbed NH_3 for determining the acidic properties of as-prepared catalysts

Catalyst	TPD analysis of absorbed NH_3 / (mmol·g^{-1})			Total evolved NH_3 / (mmol·g^{-1})	Acidic site density / (μmol·m^{-2})
	Weak (<200 ℃)	Moderate (200~450 ℃)	Strong (>450 ℃)		
SiO_2	0.28	0.43	0.25	0.96	4.96
5%Fe10%CeO_x/SiO_2-A	1.09	0.84	0.26	2.19	14.33
5%Fe10%CeO_x/SiO_2-C	0.25	0.13	0.21	0.59	3.13

2.2　Catalytic properties in reaction of prenyl acetate transesterification with methanol

The transesterification performance of the catalysts is listed in Table 4. The formation rate of prenyl alcohol in the unit of mmol product per gram of catalyst per hour (k) was also calculated and listed. It can be seen that the amorphous catalyst had much better transesterification performance than the crystalline catalyst, attributing to more basic sites.

The reaction conditions were optimized to achieve maximum yield of prenyl alcohol. The effect of temperature, the amount of catalyst and mass ratio were studied for prenyl acetate with 5%Fe10%CeO_x/SiO_2-A catalyst. The reaction temperature was varied

Table 4　Catalytic performance of as-prepared catalysts

Catalyst	Conv. of prenyl acetate[a] / %	Sel. of prenyl alcohol[a] / %	k[b] / (mmol·g^{-1}·h^{-1})
SiO_2	24.3	64.9	2.82
5%Fe10%CeO_x/SiO_2-A	95.2	96.5	16.45
5%Fe10%CeO_x/SiO_2-C	65.6	89.0	10.45

[a] Reaction conditions: $m_{methanol}/m_{prenyl\ acetate}$=9, catalyst dosage=0.48%(w/w), 130 ℃, 10 h; [b] k is the formation rate of prenyl alcohol in the unit of mmol product per gram of catalyst per hour.

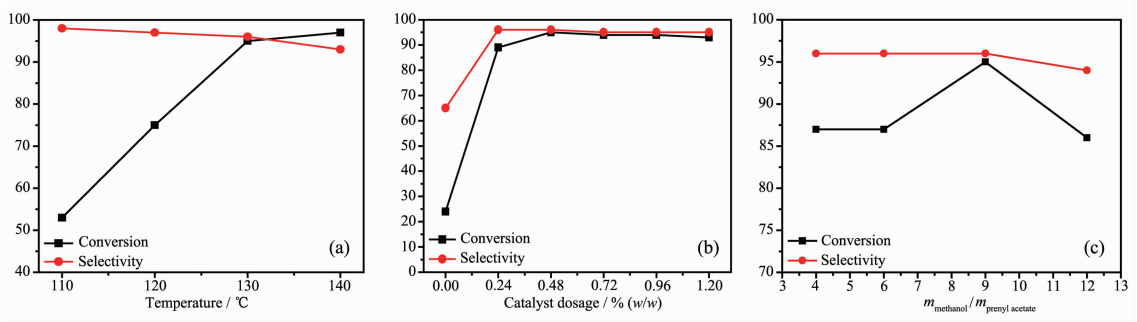

Conditions: (a) $m_{methanol}/m_{prenyl\ acetate}$=9, catalyst dosage=0.48%(*w*/*w*), reaction time=10 h; (b) $m_{methanol}/m_{prenyl\ acetate}$=9, temperature=130 ℃, reaction time=10 h; (c) catalyst dosage=0.48%(*w*/*w*), temperature=130 ℃, reaction time=10 h

Fig.8 Effect of temperature (a), catalyst dosage (b), mass ratio of methanol to prenyl acetate (c) on transesterification performance of 5%Fe10%CeO_x/SiO_2-A catalysts

from 110 to 140 ℃ and the results are shown in Fig.8 (a). The results suggested that the conversion of prenyl acetate increased with the increase in the temperature from 110 to 140 ℃. At 110 ℃, the prenyl acetate conversion was 53%, which increased to 97% upon increase in the temperature to 140 ℃. Correspondingly, the selectivity of prenyl alcohol decreased with increasing reaction temperature. The yield of prenyl alcohol was maximized at a reaction temperature of 130 ℃.

An important variable affecting the yield of prenyl alcohol was the catalyst dosage which was varied from 0 to 1.2%(*w*/*w*) keeping the temperature at 130 ℃ and $m_{methanol}/m_{prenyl\ acetate}$ of 9. Upon increasing the catalyst dosage from 0 to 1.2%, the results are shown in Fig.8(b). Hence, the catalyst dosage of 0.48%(*w*/*w*) with respect to the total reactant was found to be the optimum to get high prenyl alcohol yield.

The effect of mass ratio was studied for prenyl acetate with 0.48% (*w*/*w*) dosage of 5% Fe10% CeO_x/SiO_2-A at 130 ℃. The stoichiometry of the transesterification reaction required 1 mol of methanol per mole of prenyl acetate to yield 1 mol of methyl acetate and prenyl alcohol. To shift the transesterification reaction to the right, it was necessary to use a large excess of methanol, and hence the mass ratio of alcohol to ester was varied from 4 to 12 (Fig.8(c)). The mass ratio being 9 was considered to be the optimum mass ratio to get high conversion of prenyl acetate.

Since each experiment needed a work-up to get the conversion and yield, effect of reaction time was studied independently by carrying out transesterification for 2~20 h under the identical conditions (130 ℃, catalyst dosage =0.48% (*w*/*w*), $m_{methanol}/m_{prenyl\ acetate}$ =9) for prenyl acetate using 5% Fe10% CeO_x/SiO_2-A catalyst. The results are shown in Fig.9. With an increase in reaction time, yield of prenyl alcohol increased gradually and it remained constant after some point. From the results, it is clear that the yield hardly increases after 10 hours. Once the reaction mixture is saturated with the product, a small amount of unreacted prenyl acetate may not be able to interact with the catalyst active sites.

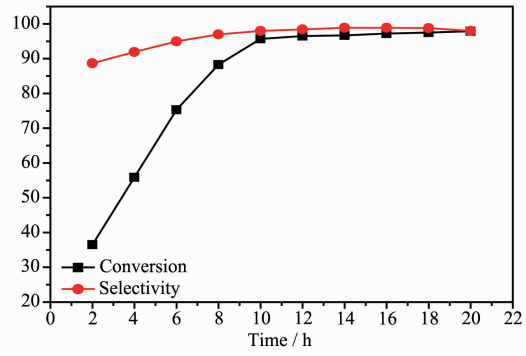

Conditions: $m_{methanol}/m_{prenyl\ acetate}$=9, catalyst dosage=0.48%(*w*/*w*), temperature=130 ℃

Fig.9 Effect of time on prenyl acetate transesterification reaction catalyzed by 5%Fe10%CeO_x/SiO_2-A catalyst

The transesterification reaction of prenyl acetate with methanol using 5%Fe10%CeO_x/SiO_2-A showed 95% conversion for 10 hours. The reusability study was conducted with 5%Fe10%CeO_x/SiO_2-A catalyst for the transesterification of prenyl acetate. The test was

performed up to 10 successive cycles for the reactions. The catalyst stayed active and showed consistent performance (Fig.10). Interestingly, the catalyst without regeneration at high temperatures was able to retain the activity after successive reuse. Furthermore, XRD patterns of both fresh and recycled catalysts for transesterification of prenyl acetate indicate that there is no change in phase purity and the amorphous structure remains stable after ten cycles (Fig.11). Iron oxide forms a stable amorphous dislocation with the cerium oxide component.

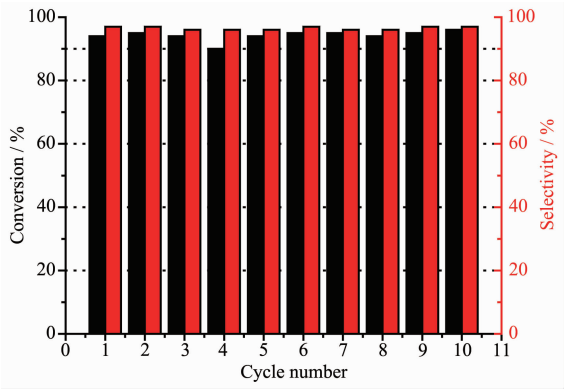

Conditions: $m_{methanol}/m_{prenyl\ acetate}$=9, catalyst dosage=0.48%(*w*/*w*), temperature=130 ℃, reaction time=10 h

Fig.10 Recyclability test of 5%Fe10CeO_x/SiO_2-A catalyst for transesterification reaction of prenyl acetate

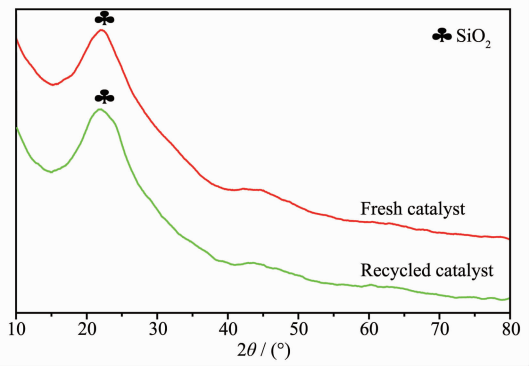

Conditions: $m_{methanol}/m_{prenyl\ acetate}$=9, catalyst dosage=0.48%(*w*/*w*), temperature=130 ℃, reaction time=10 h

Fig.11 XRD patterns of fresh and recycled 5%Fe10%CeO_x/SiO_2-A catalyst

3 Conclusions

In summary, amorphous $FeCeO_x/SiO_2$ and crystalline $FeCeO_x/SiO_2$ catalyst were obtained by chemical reduction and co-precipitation methods. For the transesterification of prenyl acetate and methanol, the high activity of 5%Fe10%CeO_x/SiO_2-A is attributed to the basicity properties. Under the optimized reaction conditions, the 5%Fe10%CeO_x/SiO_2-A catalyst offered the highest prenyl acetate conversion of 95% with an excellent prenyl alcohol selectivity of 96%. The 5%Fe10%CeO_x/SiO_2-A catalyst has more basic sites, and it has excellent stability due to the interaction of Fe and Ce. Furthermore, the catalyst remained active after 10 cycles of using, which is a composite oxide and an amorphous form. Compared with the previous reported transesterification catalysts, the $FeCeO_x/SiO_2$-A catalyst has remarkable merits in catalyst preparation, recycling and catalytic activity. Therefore, it can be inferred that the $FeCeO_x/SiO_2$-A will be of practical potential for the transesterification reaction.

Acknowledgements: The authors gratefully acknowledge the National Key Research and D&P of China (Grant No. 2017YFC0210901).

References:

[1] Xiong Z B, Lu C M, Guo D X, et al. *J. Chem. Technol. Biotechnol.*, **2013**,**88**:1258-1265

[2] Busca G. *Chem. Rev.*, **2010**,**110**:2217-2249

[3] Bhanage B M, Fujita S I, Ikushima Y, et al. *Appl. Catal. A*, **2001**,**219**:259-266

[4] Adriana M, Nadine E, Lorraine C, et al. *Appl. Catal. A*, **2013**,**468**:1-8

[5] Wang H, Wang M H, Zhao N, et al. *Catal. Lett.*, **2005**,**105**: 253-257

[6] LIU Shou-Qing(刘守庆), LI Xue-Mei(李雪梅), HE Xian-Wu (和献武), et al. *Chinese J. Inorg. Chem.*(无机化学学报), **2017**,**33**(7):1153-1160

[7] Vani V S N P, Chida A S, Srinivasan R, et al. *Synth. Commun.*, **2001**,**31**:219-224

[8] Macala G S, Robertson A W, Johnson C L, et al. *Catal. Lett.*, **2008**,**122**:205-209

[9] Baskar G, Soumiya S. *Renewable Energy*, **2016**,**98**:101-107

[10]Dhawane S H, Kumar T, Halder G. *Energy Convers. Manage.*, **2016**,**122**:310-320

[11]Suzuta T, Toba M, Abe Y. *J. Am. Oil Chem. Soc.*, **2012**,**89**: 1981-1989

[12]Hájek M, Kocík J, Frolich K, et al. *J. Cleaner Prod.*, **2017**, **161**:1423-1431

[13]Joshi G, Rawat D S, Lamba B Y. *Energy Convers. Manage.*, **2015**,**96**:258-267

[14]Shi M, Zhang P B, Fan M M. *Fuel*, **2017**,**197**:343-347

[15]Dibenedetto A, Angelini A, Bitonto L D, et al. *ChemSusChem*, **2014**,**7**:1155-1161

[16]Kumar P, Srivastava V C, Mishra I M, et al. *Renewable Energy*, **2016**,**88**:457-464

[17]Song Z W, Jin X, Hu Y F, et al. *ACS Sustainable Chem. Eng.*, **2017**,**5**:4718-4729

[18]Murugan C, Bajaj H C, Jasra R V. *Catal. Lett.*, **2010**,**137**:224-231

[19]Zhang L, Wu Y S, Bian X F, et al. *J. Non-Cryst. Solids*, **2000**,**262**:169-176

[20]MAO Dong-Sen(毛东森), GUO Qiang-Sheng(郭强胜), YU Jun(俞俊), et al. *Acta Phys.-Chim. Sin.*(物理化学学报), **2011**,**27**:2639-2645

[21]Liu J H, Yang X B, Zhang C, et al. *J. Ind. Eng. Chem.*, **2016**,**67**:1287-1293

[22]Liu W G, Wang S, Wang S D. *Appl. Catal. A*, **2016**,**510**:227-232

[23]Kurian M, Kunjachan C, Sreevalsan A. *Chem. Eng. J.*, **2017**, **308**:67-77

[24]Yamashita T, Hayes P. *Appl. Surf. Sci.*, **2008**,**254**:2441-2449

[25]Sánchez G, Dlugogorski B Z, Kennedy E M, et al. *Appl. Catal. A*, **2016**,**509**:130-142

[26]Kendelewicz T, Liu P, Doyle C S. *Surf. Sci.*, **2000**,**69**:144-163

[27]Chang L H, Sasirekha N, Chen Y W. *Ind. Eng. Chem. Res.*, **2006**,**45**:4927-4935

[28]Zou Z Q, Meng M, Guo L H, et al. *J. Hazard. Mater.*, **2009**, **163**:835-842

[29]Zhan S H, Zhang H, Zhang Y, et al. *Appl. Catal. B*, **2017**, **203**:199-209

[30]Nivangune N T, Ranade V V, Kelkar A A. *Catal. Lett.*, **2017**,**147**:2558-2569

[31]Xu J, Long K Z, Wu F, et al. *Appl. Catal. A*, **2014**,**484**:1-7

[32]Liao Y H, Li F, Pu Y F, et al. *RSC Adv.*, **2018**,**8**:785-791

[33]Hong W J, Iwanmoto S, Inoue M. *Catal. Lett.*, **2010**,**135**:190-196

[34]Rossi P F, Busca G, Lorenzelli V, et al. *Langmuir*, **1991**,**7**:2677-2681

[35]Kumar P, Srivastava V C, Mishara I M, et al. *Catal. Commun.*, **2015**,**60**:27-31